Temperature Dependence of Specific Heat Capacity of Nanostructures via Neuroevolution Machine-learned Potential

Shixian Liu,[1] Ge Zhang,[1] Fei Yin,[1] A.A. Barinov,[1] V.I. Khvesyuk,[1, a)] and Nuo Yang[2, b)]
[1)] *Department of Thermophysics, Bauman Moscow State Technical University, Moscow 105005, Russia*
[2)] *School of Science, National University of Defense Technology, Changsha 410073, China*

(Dated: 29 August 2025)

In this study, lattice dynamics calculations based on the Neuroevolution Machine-learned Potential (NEP) were performed for three types of silicon nanostructures: thin films, nanowires, and quantum dots. The temperature and size dependence of the specific heat capacity was systematically examined. The results reveal a significant enhancement in the specific heat capacity of nanostructures at low temperatures compared to bulk silicon, primarily due to phonon confinement, discrete energy spectra, and the emergence of low-frequency surface vibrational modes. These findings underscore the dominant role of nonlinear acoustic phonons at low temperatures, with increasing contributions from optical modes as the temperature rises. Notably, this work reports the temperature-dependent evolution of local fitting exponents in the specific heat scaling relation $C_v \sim T^{n(T)}$ for nanostructured systems. The high accuracy and computational efficiency of the NEP model allow for detailed characterization of the complex phonon behaviors that govern thermal properties at the nanoscale.

I. INTRODUCTION

The temperature dependence of specific heat at low temperatures plays a critical role in emerging technologies such as quantum computing and deep space exploration[1]. As a fundamental thermal property, specific heat governs energy storage and thermal response. In quantum computing, nanostructured materials may exhibit unusually high specific heat at millikelvin temperatures[2,3], leading to increased thermal excitations that shorten qubit coherence times and reduce readout accuracy. In cryogenic space applications, where temperatures approach absolute zero, nanocoatings are employed to regulate heat flow. However, elevated specific heat can compromise thermal buffering, potentially destabilizing control systems[4,5].

A comprehensive understanding of phonon dynamics and specific heat in nanostructures is critical for advancing thermal management strategies and optimizing the performance of next-generation nanoelectronic and quantum devices. Over the past two decades, nanostructures such as thin films, nanowires, and quantum dots have been extensively developed and have become integral components of modern electronic and photonic systems. While both electrical and thermal transport properties are of considerable interest[6–8], the thermal behavior—particularly the specific heat—of nanoscale systems often deviates substantially from that of bulk materials due to pronounced confinement and surface effects[8–11].

Experimental observations have consistently reported enhanced specific heat in nanostructures at low temperatures. Novotny and Meincke[12,13] observed a marked increase in the specific heat of lead and indium nanoparticles as small as 2.2 nm in the 1.5–15 K range. Similar enhancements were reported in palladium and vanadium powders with particle sizes below 10 nm, though the presence of structural disorder and surface oxidation introduces additional complexity in interpreting the results[14].

On the theoretical front, studies of specific heat in nanostructures are primarily based on phonon dispersion and density of states (DOS) calculations. Wang et al.[15] employed an elastic continuum model that incorporates a weighted combination of Einstein and Debye vibrational modes to assess the size and surface effects on the specific heat of nanoparticles. McNamara et al.[16] investigated discrete vibrational modes in low-dimensional lattices, replacing the Debye integral with a directional summation while still assuming linear dispersion. Their results indicated that at low temperatures, the specific heat of nanostructures is suppressed relative to bulk, in contrast to experimental observations.

Huang et al.[17] addressed this inconsistency by solving elastic wave equations in confined directions to obtain discrete vibrational modes, and integrating over continuous directions for in-plane modes. This approach led to the formulation of a low-dimensional Debye model, where contributions from dilatational, flexural, and shear waves were analyzed individually.

Using the dynamical matrix method with free boundary conditions, Pascual-Gutiérrez et al.[18] modeled the phonon modes of confined silicon structures under the harmonic approximation with environment-dependent potentials. Their findings indicated that for silicon (111) thin films, size effects on specific heat vanish when the thickness exceeds 10 nm, while for nanowires, the corresponding threshold is around 5 nm. These size effects were found to be most pronounced in the low-temperature regime.

Roslee et al.[19] employed density functional theory (DFT) to investigate the heat capacity of quantum dots. By analyzing modifications in the phonon density of states and considering elastic coupling of atomic vibrations, they proposed a $T^{3/2}$ scaling model for specific heat, which was later extended to nanofilms and nanowires[20]. The present authors have also previously explored temperature fluctuations in quantum dots

[a)] Email: khvesyuk@bmstu.ru
[b)] Email: nuo@nudt.edu.cn

based on these results[21]. However, that analysis did not account for the discrete nature of phonon modes in confined systems, where allowed wavelengths are constrained such that the system size equals an integer multiple of half the wavelength.

DFT is currently one of the most accurate computational methods at the atomic scale. However, its high computational cost makes it impractical for systems containing a large number of atoms. In contrast, traditional empirical potentials[22] offer high computational efficiency but often suffer from limited accuracy due to their fixed functional forms and small number of fitting parameters. In recent years, machine-learned interatomic potentials have emerged as a powerful alternative, combining the accuracy of first-principles methods with the efficiency of empirical models. In particular, the Neuroevolution Machine-learned Potential (NEP), developed based on neuroevolution strategies, has been widely adopted in a range of applications—including thermal transport—due to its combination of high accuracy and computational efficiency[23–26].

In this study, lattice dynamics simulations are performed for three classes of nanostructures—thin films, nanowires, and quantum dots—using the NEP model, a pre-trained machine-learned potential developed using training data from ab initio calculations of silicon[27]. The size- and temperature-dependent behavior of specific heat is systematically analyzed across low to intermediate temperature ranges. For quantum dot systems, the specific heat is obtained through summation over discrete energy levels. Notably, the temperature evolution of the local fitting exponent in the relation $C_v \sim T^{n(T)}$ is reported for the first time, providing new insights into the complex thermal behavior of nanostructured materials, enabled by the high accuracy of machine-learning-based potentials.

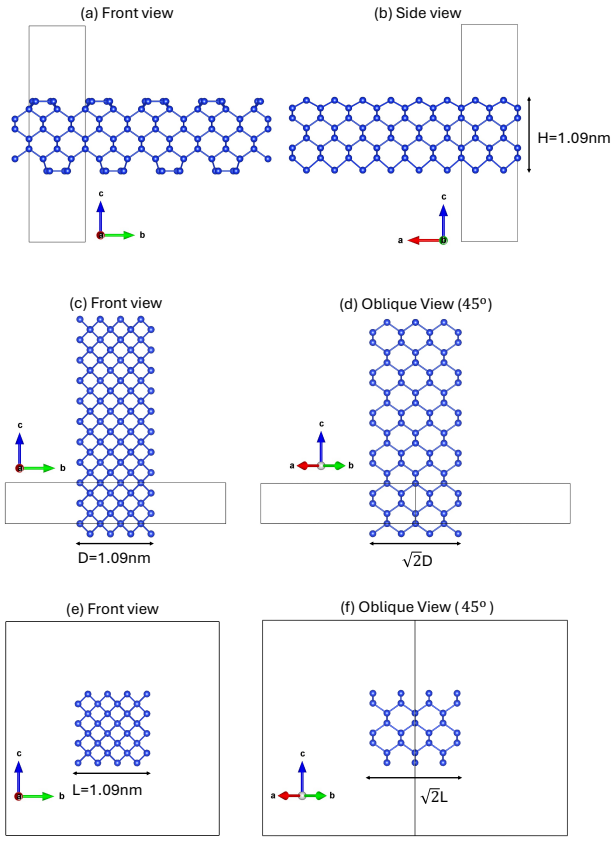

FIG. 1. (a) Front view and (b) side view of the unit cell for the silicon thin film with a thickness H=1.09 nm and 2×2 surface reconstruction; (c) front view and (d) 45-degree oblique view of the unit cell for the silicon nanowire with a square cross-sectional width D=1.09 nm; (e) front view and (f) 45-degree oblique view of the full structure of the cubic silicon quantum dot with a side length L=1.09 nm.

II. MODEL AND METHODOLOGY

As illustrated in Figure 1, the unit cells of three representative silicon nanostructures — (a, b) thin films with thickness H, (c, d) nanowires with square cross-sectional width D, and (e, f) quantum dots with side length L — are constructed for lattice dynamics calculations. The size of the unit cell along the periodic direction for the thin film is twice that of the primitive unit cell of bulk silicon, whereas for the nanowire it is identical to that of the conventional bulk unit cell. Vacuum layers are applied along the confined directions to eliminate interactions between periodic images. The configurations shown correspond to the initial, unrelaxed atomic structures. Upon structural optimization (relaxation), surface atoms rearrange to reach the lowest-energy stable configurations, consistent with previous theoretical studies[28,29]. The structural stability is preliminarily verified by confirming the absence of imaginary phonon frequencies in the dispersion relations. To further assess the accuracy of the NEP potential, Appendix A provides a comparison between the phonon dispersion relations of a ∼1 nm thick silicon film obtained using NEP model and those calculated from DFT.

Lattice Dynamics in Reciprocal Space is well suited for periodic systems such as bulk crystals, thin films, and nanowires, where translational symmetry allows the use of phonon wavevectors within the Brillouin zone. This approach significantly reduces the computational cost by diagonalizing the dynamical matrix at a finite number of k-points. Lattice Dynamics in Real Space, on the other hand, is required for quantum dots, which lack translational symmetry. In such finite systems, the entire force constant matrix must be constructed and diagonalized in real space to obtain discrete vibrational modes.

A. Lattice Dynamics in Reciprocal Space

The analysis begins with the equation of motion under the harmonic approximation:

$$m_k \ddot{u}_\alpha(\boldsymbol{l},k,t) = -\sum_{\boldsymbol{l}',k',\beta} \Phi_{\alpha\beta}(\boldsymbol{l}k,\boldsymbol{l}'k') u_\beta(\boldsymbol{l}',k',t). \quad (1)$$

Here, $\boldsymbol{l}$ denotes the lattice vector identifying the position of a unit cell in the crystal, and k indexes atoms within the unit

cell, where $k = 1,2,\ldots,s$ for s atoms per unit cell. The indices α and β represent Cartesian components (x, y, z), and $\Phi_{\alpha\beta}(\boldsymbol{l}k,\boldsymbol{l}'k')$ are the components of the interatomic force constant matrix, describing the interaction between atom k in cell $\boldsymbol{l}$ and atom k' in cell $\boldsymbol{l}'$.

Assuming a Bloch-wave solution of the form

$$u_\alpha(\boldsymbol{l},k,t) = \frac{1}{\sqrt{m_k}} e^{i(\boldsymbol{q}\cdot\boldsymbol{l}-\omega t)} A_\alpha(k,\boldsymbol{q}), \tag{2}$$

and utilizing translational symmetry, such that $\Phi_{\alpha\beta}(\boldsymbol{l}k,\boldsymbol{l}'k') = \Phi_{\alpha\beta}(k,k';\boldsymbol{R})$ with $\boldsymbol{R} = \boldsymbol{l}' - \boldsymbol{l}$, the phonon eigenvalue problem is obtained:

$$\omega^2(\boldsymbol{q})A_\alpha(k,\boldsymbol{q}) = \sum_{k',\beta} D_{\alpha\beta}(k,k';\boldsymbol{q})A_\beta(k',\boldsymbol{q}), \tag{3}$$

where the dynamical matrix is defined as

$$D_{\alpha\beta}(k,k';\boldsymbol{q}) = \frac{1}{\sqrt{m_k m_{k'}}} \sum_{\boldsymbol{R}} \Phi_{\alpha\beta}(k,k';\boldsymbol{R}) e^{i\boldsymbol{q}\cdot\boldsymbol{R}}. \tag{4}$$

In matrix notation, the eigenvalue equation becomes:

$$\mathbf{D}(\boldsymbol{q})\cdot\boldsymbol{A}(\boldsymbol{q}) = \omega^2(\boldsymbol{q})\cdot\boldsymbol{A}(\boldsymbol{q}). \tag{5}$$

For each wave vector $\boldsymbol{q}$ in the first Brillouin zone, this eigenvalue problem yields $3s$ phonon branches, where s is the number of atoms per unit cell and the factor of 3 accounts for the three degrees of freedom per atom.

The lattice specific heat at constant volume is given by

$$C_v(T) = \frac{1}{V}\sum_s \sum_{\boldsymbol{q}} \hbar\omega_{\boldsymbol{q},s} \frac{\partial f_{\mathrm{BE}}(\omega_{\boldsymbol{q},s},T)}{\partial T}, \tag{6}$$

where $f_{\mathrm{BE}}(\omega,T)$ denotes the Bose-Einstein distribution function.

To simplify the summation, the expression can be transformed into an integral over phonon frequencies by introducing the phonon density of states $\mathrm{DOS}(\omega)$:

$$C_v(T) = \int_0^{\omega_{\max}} \hbar\omega \frac{\partial f_{\mathrm{BE}}(\omega,T)}{\partial T} \mathrm{DOS}(\omega)\, d\omega. \tag{7}$$

Here, $\mathrm{DOS}(\omega)$ is defined as:

$$\mathrm{DOS}(\omega) = \frac{1}{V}\sum_{q,s} \delta(\omega - \omega_{q,s}),. \tag{8}$$

where the summation is over all q-points in the Brillouin zone and all phonon branches s, and δ is the Dirac delta function.

B. Lattice Dynamics in Real Space

Quantum dots, being finite systems without translational symmetry, require a real-space formulation. For an N-atom system, the equation of motion for each atom i in Cartesian direction α is expressed as:

$$m_i \ddot{u}_i^\alpha(t) = -\sum_{j,\beta} \Phi_{\alpha\beta}(i,j) u_j^\beta(t), \tag{9}$$

where $\Phi_{\alpha\beta}(i,j)$ are the elements of the force constant matrix describing interactions between components α and β of atoms i and j, respectively. The full matrix $\mathbf{H}$, assembled from all such elements, is symmetric and of size $3N \times 3N$.

Assuming a harmonic time dependence $u_i^\alpha(t) = A_i^\alpha e^{i\omega t}$ and substituting into Eq. (8), the following eigenvalue equation is obtained:

$$m_i\omega^2 A_i^\alpha = -\sum_{j,\beta} \Phi_{\alpha\beta}(i,j) A_j^\beta. \tag{10}$$

This can be written in matrix form as:

$$\mathbf{M}^{-1}\mathbf{H}\cdot\boldsymbol{A}_n = \omega_n^2\cdot\boldsymbol{A}_n, \tag{11}$$

where $\mathbf{M}$ is a diagonal mass matrix with entries $M_{ii} = m_i$, and $\boldsymbol{A}_n$ is the polarization vector corresponding to the n-th normal mode with frequency ω_n.

Solving this generalized eigenvalue problem yields $3N$ discrete vibrational modes, which constitute the vibrational spectrum of the finite system. Since periodicity is not introduced in this approach, the wave vector $\boldsymbol{q}$ is absent, and the expression for the specific heat capacity in Eq. (6) becomes a summation over the discrete set of eigenfrequencies:

$$C_v(T) = \frac{1}{V}\sum_{n=1}^{3N} \hbar\omega_n \frac{\partial f_{\mathrm{BE}}(\omega_n,T)}{\partial T}. \tag{12}$$

This formulation is particularly suitable for systems without translational symmetry, such as nanoclusters, molecules, and quantum dots.

C. Computational Details

The total energies and atomic forces of the optimized silicon nanostructures were calculated using the NEP model[30]. The harmonic force constants were subsequently extracted via the finite displacement method implemented in the PHONOPY package[31].

For bulk silicon, thin films, and nanowires, the real-space force constants were transformed into reciprocal space to construct the dynamical matrix, and the phonon frequencies were obtained by solving the corresponding eigenvalue problem. In contrast, for quantum dots, which lack translational symmetry, the eigenvalues of the full real-space force constant matrix were computed directly.

For a quantum dot containing 64 atoms (L=1.09 nm), the calculation takes approximately 2 seconds; For 512 atoms (L=2.17 nm), it takes about 56 seconds; For 1728 atoms (L=3.26 nm), the calculation requires approximately 105 minutes.

After determining the phonon frequencies, the phonon density of states and the temperature-dependent specific heat capacity were calculated through statistical sampling of the vibrational spectrum.

III. RESULTS AND DISCUSSION

Figure 2 presents the temperature-dependent specific heat capacity of silicon nanostructures with varying geometries, including thin films of different thicknesses H, nanowires with square cross-sectional widths D, and quantum dots of side lengths L. Across all nanostructures, a consistent enhancement in specific heat capacity is observed at low temperatures compared to bulk silicon. Furthermore, this enhancement becomes increasingly pronounced as the structural size decreases. This behavior is attributed to the dominant contribution of long-wavelength, low-frequency phonons in confined systems (see Figure 3), which play a significant role in thermal properties at low temperatures.

The Debye model assumes a linear phonon dispersion, leading to a quadratic phonon DOS. As a result, the specific heat exhibits a cubic temperature dependence at low temperatures, as shown by the black dashed line in Figure 2. The red markers represent the experimental data of bulk silicon's specific heat, which show excellent agreement with the NEP model calculations presented in this work.

The underlying mechanisms can be further elucidated by analyzing the phonon DOS, as shown in Figure 3. For thin films with a thickness of approximately 1 nm (Figure 3a) and nanowires with lateral dimensions around 1 nm (Figure 3b), multiple peaks emerge due to internal standing waves and surface phonon modes. In the case of quantum dots (Figure 3c), the vibrational spectrum becomes fully discrete as a result of strong confinement, with the density of discrete frequencies qualitatively representing the DOS, even though individual frequency values lack direct physical significance.

The observed enhancement in low-temperature specific heat can also be understood from a dimensionality perspective. As illustrated in Figures 2a–c, structures of lower dimensionality exhibit higher specific heat at low temperatures. This trend is consistent with the predictions of the extended Debye model for low-dimensional systems[17], which suggests scaling laws of $C_v \propto T^2$ for two-dimensional structures and $C_v \propto T$ for one-dimensional systems in the low-temperature limit.

However, both the classical Debye model and its extended forms assume purely linear acoustic dispersion and neglect optical branches, which limits their accuracy. In contrast, the present study fully incorporates the actual nonlinear acoustic branches—particularly important at low temperatures—as well as optical branches, which contribute significantly at intermediate and high temperatures. This comprehensive treatment allows for a more accurate description of the specific heat behavior across a wide temperature range.

In addition to the confinement effects observed in nanostructures, bulk silicon also exhibits deviations from the Debye model, as shown in Figure 2. At low temperatures, these deviations arise from the inclusion of nonlinear acoustic branches in our calculations, while the Debye model assumes linear dispersion. At intermediate temperatures, optical branches—neglected by the Debye approximation—become increasingly important. As the temperature approaches zero, the contribution of only long-wavelength acoustic phonons near the Γ point remains, which exhibit nearly linear dispersion; consequently, the Debye model becomes valid in this regime.

To further quantify the low-temperature behavior, we extract the temperature-dependent fitting exponent n from the relation $C_v \sim T^{n(T)}$, as shown in Figures 2d–f. The exponent was determined through local fits over five-point temperature intervals. Validation tests confirmed that using fitting windows ranging from 3 to 20 temperature points yields nearly identical results, indicating that the choice of window size has negligible influence on the extracted values. Notably, for nanostructures, n does not stabilize even at very low temperatures. This is due to the persistence of nonlinear dispersion near the Γ point arising from flexural modes.

In low-dimensional systems such as thin films and nanowires, flexural phonon modes exhibit nonlinear dispersion near the Γ point. This deviation from linear behavior leads to a density of states (DOS) that no longer follows a simple power-law form. Consequently, the integral expression for the specific heat does not yield a constant temperature exponent. As the temperature increases, phonons across a wider range of frequencies are thermally excited, effectively allowing the system to "sample" different regions of the dispersion relation. This results in a temperature-dependent heat capacity of the form $C_v(T) \sim T^{n(T)}$, where the exponent $n(T)$ is no longer constant but evolves with temperature.

To the best of our knowledge, the temperature dependence of the exponent n is systematically presented here for the first time. In all cases, n increases with temperature, reaches a peak around 20 K, and subsequently decreases. For example, for a film with a thickness of approximately 1 nm, n increases from 1.5 at low temperatures to about 3 at 20 K before decreasing. For films thicker than 2 nm, n exceeds 3 at 20 K. For a nanowire with a lateral size of 1 nm, n rises from 1 to approximately 2 at 20 K. In the case of a 1 nm quantum dot, n increases from 0.5 to around 1.5. For comparison, the curve for bulk silicon is also provided, demonstrating that as the structural size increases, the behavior of nanostructures gradually converges toward that of the bulk.

The non-monotonic behavior of the exponent $n(T)$ results from the sequential thermal activation of different phonon modes. At low temperatures, specific heat is primarily governed by low-frequency flexural modes with nonlinear dispersion, leading to a small value of $n(T)$. As the temperature increases, phonon modes with steeper dispersion become thermally active, causing $n(T)$ to rise. At even higher temperatures, high-frequency optical modes with flatter dispersion start to contribute. Since these modes exhibit weaker temperature dependence, they reduce the rate of growth of the specific heat, resulting in a gradual decrease in $n(T)$ at elevated temperatures.

Since thermal conductivity is proportional to the product of specific heat, phonon group velocity, and phonon mean free path, the temperature dependence of specific heat can significantly affect thermal transport—particularly at low temperatures, where deviations from bulk behavior are more pronounced in low-dimensional systems. However, in nanostructures, quantum confinement and size effects significantly re-

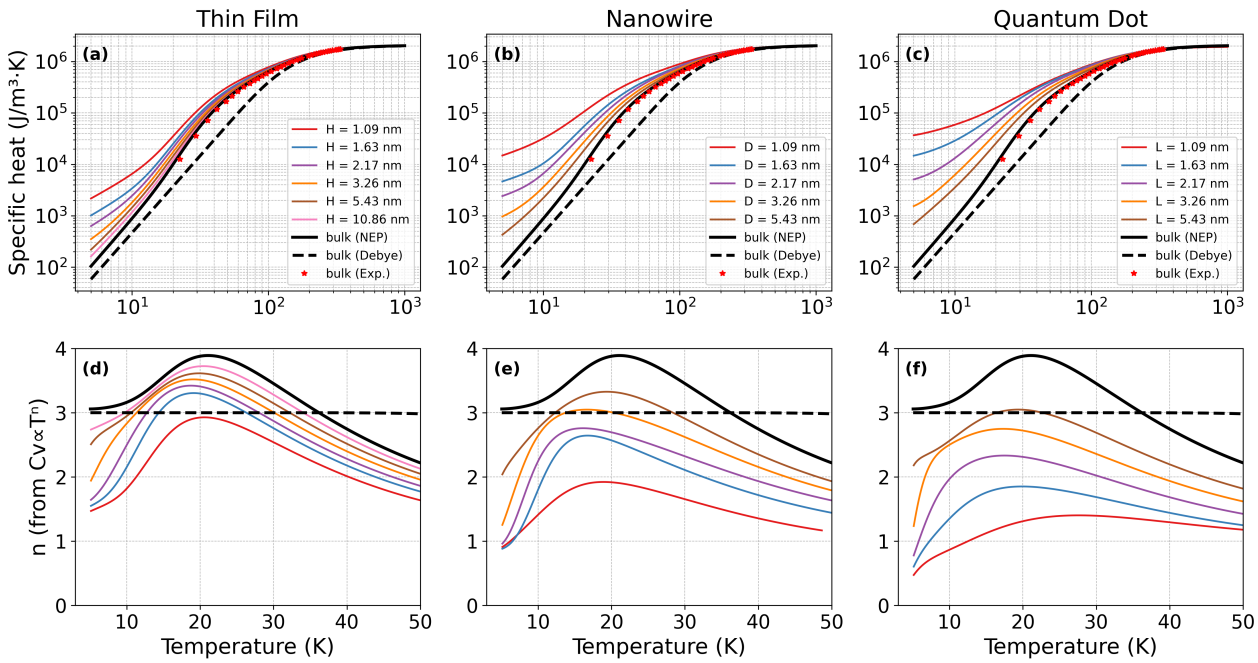

FIG. 2. (a–c) Temperature dependence of the specific heat capacity for silicon nanostructures of various sizes, along with bulk results obtained using the NEP model, Debye model, and experimental data, and (d–f) the corresponding temperature-dependent fitting exponent n in the relation $C_v \sim T^n$. Specifically, (a, d) show results for thin films with different thickness H; (b, e) for nanowires with different square cross-sectional widths D; and (c, f) for quantum dots with different side lengths L.

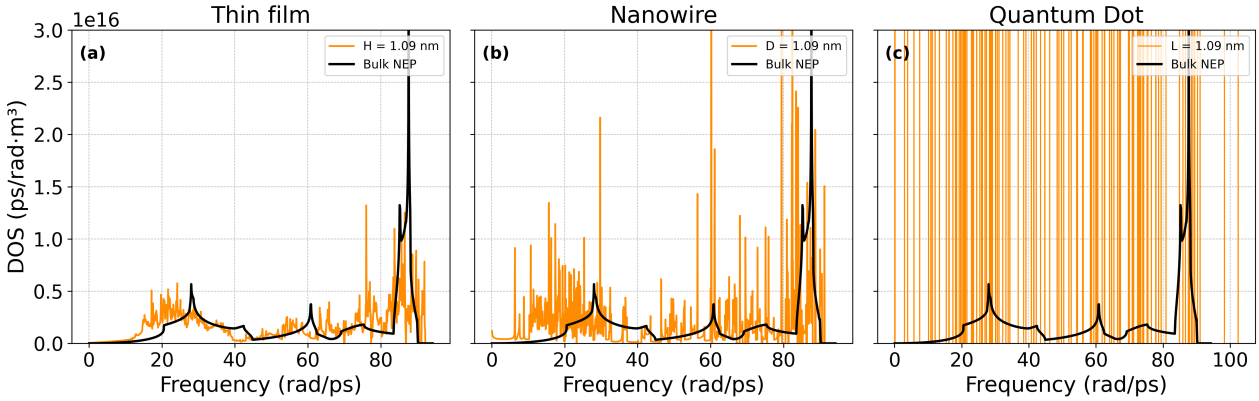

FIG. 3. Phonon density of states (DOS) for different nanostructures: (a) thin film with a thickness of 1.09 nm, (b) nanowire with a square cross-section of width 1.09 nm, and (c) quantum dot with a side length of 1.09 nm, compared with bulk silicon.

duce both phonon group velocity and mean free path[32]. As a result, the enhancement in specific heat may not necessarily lead to an increase in thermal conductivity.

To ensure numerical accuracy, convergence tests were performed for both the Brillouin zone mesh density and the frequency bin width used in the DOS calculations. Figures 4a and 4c show that a $120 \times 120 \times 120$ grid yields fully converged results, even at very low temperatures. Similarly, Figures 4b and 4d demonstrate that a frequency bin width of 0.05 THz is sufficiently fine to ensure reliable accuracy in the specific heat calculations.

For bulk silicon, the fitting exponent n also reaches a maximum near 20 K, indicating the most rapid variation in specific heat with temperature. Below 40 K, n exceeds the Debye value of 3, reflecting a steeper increase. As the temperature further decreases, n gradually approaches 3. Above 40 K, n falls below 3, indicating a saturation trend. At high temperatures, the specific heat approaches a constant value, corresponding to $n \approx 0$.

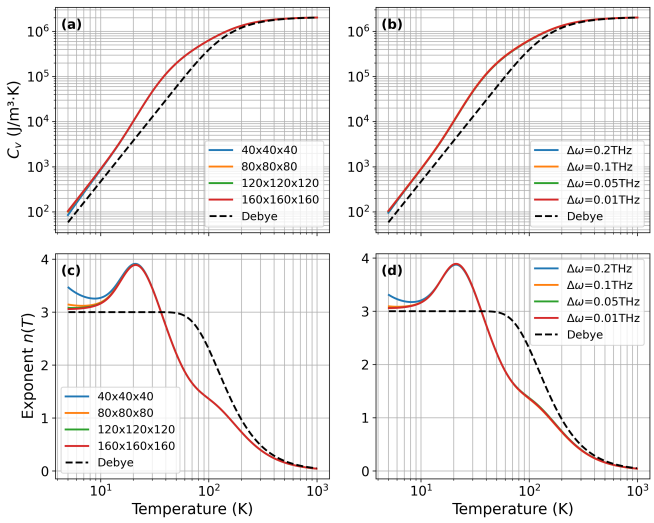

FIG. 4. Convergence tests for heat capacity calculations of bulk silicon.

IV. CONCLUSION

In this work, the temperature- and size-dependent specific heat capacity of silicon nanostructures at low and intermediate temperatures was systematically investigated using the NEP framework. The results clearly demonstrate that, due to phonon confinement, discrete energy levels, and the presence of low-frequency surface phonon modes, all nanostructures exhibit an enhanced specific heat capacity at low temperatures compared to bulk silicon, with this enhancement becoming more pronounced as the structural size decreases.

The analysis reveals that nonlinear acoustic branches dominate the thermal behavior at low temperatures, while optical phonon branches contribute significantly at intermediate and higher temperatures. Notably, this study presents, for the first time, the temperature-dependent evolution of the local fitting exponent n in the relation $C_v \sim T^n$ for various nanostructures. The application of a machine-learning-based interatomic potential enables accurate and detailed characterization of the phonon spectrum, capturing the intricate and nontrivial temperature dependence of specific heat capacity. Although silicon was used as the model system in this work, the methodology and the key findings regarding the temperature-dependent specific heat capacity and the evolution of $n(T)$ are general and can be extended to other nanostructured materials with similar phonon confinement effects.

These findings provide important insights into the thermal properties of low-dimensional systems and underline the relevance of $n(T)$ to quantum thermal management and nanoscale heat capacity engineering, where controlling the temperature dependence of specific heat can enable optimized thermal energy storage, transfer, and dissipation at the nanoscale. They offer valuable guidance for the design and optimization of nanoscale devices with tailored thermal management characteristics.

ACKNOWLEDGMENTS

S. Liu and F. Yin gratefully acknowledges financial support from the China Scholarship Council (No. 202308090243 for S. Liu and No. 202408090635 for F. Yin).

CONFLICT OF INTEREST STATEMENT

The authors have no conflicts to disclose.

DATA AVAILABILITY STATEMENT

The data and scripts supporting the findings of this study are available at: `https://github.com/lyushisyan/NEP-specific-heat`.

Appendix A: Validation of NEP

To evaluate the accuracy and reliability of the NEP model in predicting phonon-related thermal properties, we compare the phonon dispersion, DOS, and specific heat obtained using NEP with those from first-principles DFT calculations. As shown in Figure 5, both methods produce generally consistent results for a silicon thin film with a thickness of 1.09 nm, confirming that NEP is capable of efficiently and accurately simulating the lattice dynamics of low-dimensional silicon nanostructures.

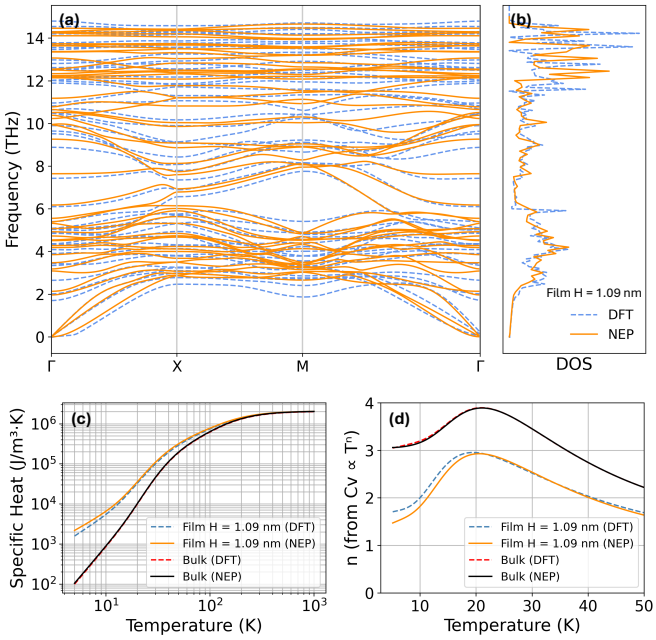

FIG. 5. Comparison of phonon dispersion relations and density of states for a silicon thin film approximately 1 nm thick, obtained using the NEP and DFT.

Although there are some noticeable deviations in the phonon dispersion curves—particularly for acoustic phonons near the Γ point—we emphasize that this discrepancy has limited impact on the thermal properties of interest. Figures 5c and 5d show that the specific heat of bulk silicon computed using NEP closely matches the DFT result. For the 1.09 nm film, the specific heat values from NEP and DFT are also in good agreement, with only minor differences. Moreover, the temperature dependence of the effective exponent $n(T)$, obtained from the power-law relation $C_v \sim T^{n(T)}$, exhibits similar trends for both methods. These findings support the conclusion that the NEP model remains reliable for capturing the key thermal behaviors discussed in this work.

Appendix B: Detailed Dispersion Analysis

The phonon dispersion relation of the 2.17-nm-thick film and a close-up near the Γ point are shown in Figure 6. In the zoomed-in view, three acoustic branches can be identified: two with linear dispersion and one with quadratic dispersion. These correspond to shear horizontal (SH), longitudinal (L), and flexural (F) modes, respectively. The flexural mode typically emerges in thin films with small thicknesses.

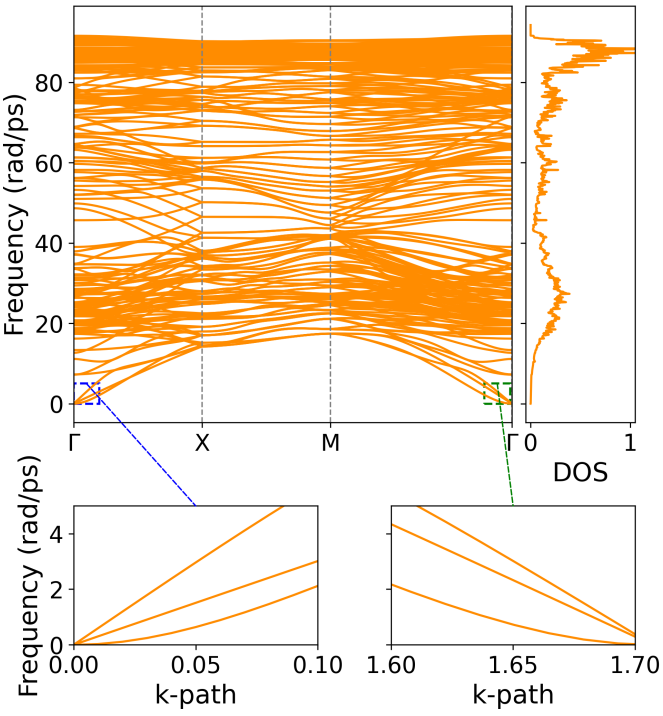

FIG. 6. The phonon dispersion relation of the 2.17-nm-thick film and a close-up near the Γ point.

Appendix C: Analysis at different temperatures

Figure 7 shows the normalized cumulative specific heat capacity for silicon thin films and bulk (NEP model and Debye model) at various temperatures. At low temperatures, the specific heat capacity is dominated by low-frequency, long-wavelength phonons, which are predominantly acoustic. As the temperature increases, higher-frequency phonons increasingly contribute to the heat capacity. Notably, at T = 10 K, the bulk heat capacity from the NEP model closely matches that from the Debye model, whereas at T = 20 K, a significant deviation appears, indicating that optical modes start to play a non-negligible role from around 20 K.

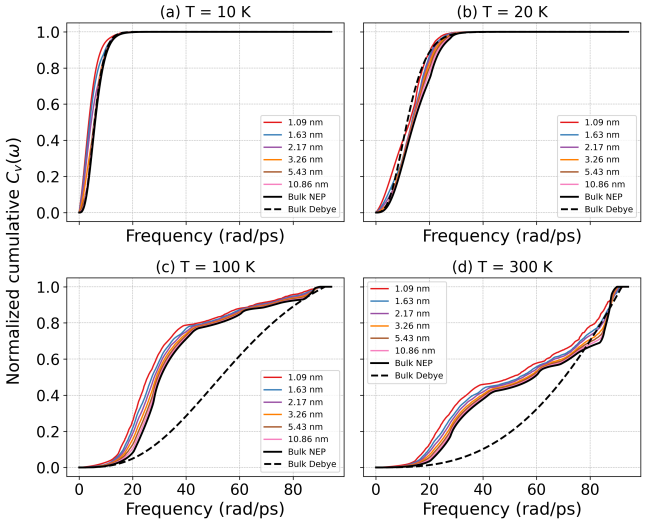

FIG. 7. Normalized cumulative specific heat capacity of thin films and bulk (NEP model and Debye model) at different temperatures

[1] F. Pobell, *Matter and methods at low temperatures*, 3rd ed. (Springer, Berlin ; New York, 2007).

[2] J. M. Martinis, S. Nam, J. Aumentado, and C. Urbina, "Rabi Oscillations in a Large Josephson-Junction Qubit," Physical Review Letters **89**, 117901 (2002).

[3] F. Giazotto, T. T. Heikkilä, A. Luukanen, A. M. Savin, and J. P. Pekola, "Opportunities for mesoscopics in thermometry and refrigeration: Physics and applications," Reviews of Modern Physics **78**, 217–274 (2006).

[4] J. Doty, K. Yerkes, L. Byrd, J. Murthy, A. Alleyne, M. Wolff, S. Heister, and T. S. Fisher, "Dynamic Thermal Management for Aerospace Technology: Review and Outlook," Journal of Thermophysics and Heat Transfer **31**, 86–98 (2017).

[5] R. C. Youngquist, M. A. Nurge, W. L. Johnson, T. L. Gibson, and J. M. Surma, "Cryogenic Deep Space Thermal Control Coating," Journal of Spacecraft and Rockets **55**, 622–631 (2018).

[6] N. Yang, G. Zhang, and B. Li, "Violation of Fourier's law and anomalous heat diffusion in silicon nanowires," Nano Today **5**, 85–90 (2010).

[7] Y. Ma, "Size-dependent thermal conductivity in nanosystems based on non-Fourier heat transfer," Applied Physics Letters **101**, 211905 (2012).

[8] S.-X. Liu, A. A. Barinov, F. Yin, and V. I. Khvesyuk, "Determination of thermal properties of unsmooth Si-nanowires," Chinese Physics Letters **41**, 016301 (2024).

[9] I. Ponomareva, D. Srivastava, and M. Menon, "Thermal Conductivity in Thin Silicon Nanowires: Phonon Confinement Effect," Nano Letters **7**, 1155–1159 (2007).

[10]T. Tong, R. Prasher, and A. Majumdar, "Heat Capacity and Thermal Conductance Calculations for Non-Metallic Crystalline Nanowires Based on Elastic Dispersion Relations," in *Volume 11: Micro and Nano Systems, Parts A and B* (ASMEDC, Seattle, Washington, USA, 2007) pp. 631–637.
[11]R. Prasher, T. Tong, and A. Majumdar, "Approximate Analytical Models for Phonon Specific Heat and Ballistic Thermal Conductance of Nanowires," Nano Letters **8**, 99–103 (2008).
[12]V. Novotny, P. P. M. Meincke, and J. H. P. Watson, "Effect of Size and Surface on the Specific Heat of Small Lead Particles," Physical Review Letters **28**, 901–903 (1972).
[13]V. Novotny and P. P. M. Meincke, "Thermodynamic Lattice and Electronic Properties of Small Particles," Physical Review B **8**, 4186–4199 (1973).
[14]O. Vergara, D. Heitkamp, and H. Löhneysen, "Specific heat of small vanadium particles in the normal and superconducting state," Journal of Physics and Chemistry of Solids **45**, 251–258 (1984).
[15]B.-X. Wang, L.-P. Zhou, and X.-F. Peng, "Surface and Size Effects on the Specific Heat Capacity of Nanoparticles," International Journal of Thermophysics **27**, 139–151 (2006).
[16]A. J. McNamara, B. J. Lee, and Z. M. Zhang, "Quantum Size Effect on the Lattice Specific Heat of Nanostructures," Nanoscale and Microscale Thermophysical Engineering **14**, 1–20 (2010).
[17]M.-J. Huang, T.-M. Chang, C.-K. Liu, and C.-K. Yu, "A theoretical study of the specific heat and Debye temperature of low-dimensional materials," International Journal of Heat and Mass Transfer **51**, 4470–4479 (2008).
[18]J. A. Pascual-Gutiérrez, J. Y. Murthy, and R. Viskanta, "Limits of size confinement in silicon thin films and wires," Journal of Applied Physics **102**, 034315 (2007).
[19]A. E. Roslee, S. K. Muzakir, J. Ismail, M. M. Yusoff, and R. Jose, "A heat capacity model of $T^{3/2}$ dependence for quantum dots," Physical Chemistry Chemical Physics **19**, 408–418 (2017).
[20]A. E. Roslee, N. A. Nik Mohamed, P. Thamburaja, and R. Jose, "A generalized thermophysical model for materials from molecular clusters to bulk crystals," Physica B: Condensed Matter **659**, 414877 (2023).
[21]S. Liu and V. I. Khvesyuk, "Temperature fluctuations in quantum dots: Insights from a T3/2 heat capacity model," Physics Letters A **534**, 130261 (2025).
[22]J. Tersoff, "Modeling solid-state chemistry: Interatomic potentials for multicomponent systems," Physical review B **39**, 5566 (1989).
[23]Z. Fan, Z. Zeng, C. Zhang, Y. Wang, K. Song, H. Dong, Y. Chen, and T. Ala-Nissila, "Neuroevolution machine learning potentials: Combining high accuracy and low cost in atomistic simulations and application to heat transport," Physical Review B **104**, 104309 (2021).
[24]K. Song, R. Zhao, J. Liu, Y. Wang, E. Lindgren, Y. Wang, S. Chen, K. Xu, T. Liang, P. Ying, *et al.*, "General-purpose machine-learned potential for 16 elemental metals and their alloys," Nature Communications **15**, 10208 (2024).
[25]X. Wu, Z. Wu, T. Liang, Z. Fan, J. Xu, M. Nomura, and P. Ying, "Phonon coherence and minimum thermal conductivity in disordered superlattices," Physical Review B **111**, 085413 (2025).
[26]T. Liang, K. Xu, E. Lindgren, Z. Chen, R. Zhao, J. Liu, E. Berger, B. Tang, B. Zhang, Y. Wang, K. Song, P. Ying, N. Xu, H. Dong, S. Chen, P. Erhart, Z. Fan, T. Ala-Nissila, and J. Xu, "Nep89: Universal neuroevolution potential for inorganic and organic materials across 89 elements," (2025), arXiv:2504.21286 [cond-mat.mtrl-sci].
[27]A. P. Bartók, J. Kermode, N. Bernstein, and G. Csányi, "Machine learning a general-purpose interatomic potential for silicon," Phys. Rev. X **8**, 041048 (2018).
[28]K. D. Brommer, M. Needels, B. Larson, and J. D. Joannopoulos, "*Ab initio* theory of the Si(111)-(7×7) surface reconstruction: A challenge for massively parallel computation," Physical Review Letters **68**, 1355–1358 (1992).
[29]A. Ramstad, G. Brocks, and P. J. Kelly, "Theoretical study of the Si(100) surface reconstruction," Physical Review B **51**, 14504–14523 (1995).
[30]Z. Fan, Y. Wang, P. Ying, K. Song, J. Wang, Y. Wang, Z. Zeng, K. Xu, E. Lindgren, J. M. Rahm, A. J. Gabourie, J. Liu, H. Dong, J. Wu, Y. Chen, Z. Zhong, J. Sun, P. Erhart, Y. Su, and T. Ala-Nissila, "GPUMD: A package for constructing accurate machine-learned potentials and performing highly efficient atomistic simulations," The Journal of Chemical Physics **157**, 114801 (2022).
[31]A. Togo, "First-principles Phonon Calculations with Phonopy and Phono3py," Journal of the Physical Society of Japan **92**, 012001 (2023).
[32]S. Liu, Z. Zong, F. Yin, V. Khvesyuk, and N. Yang, "Quantifying particle and wave effects in phonon transport of pillared graphene nanoribbons," International Journal of Thermal Sciences **217**, 110067 (2025).